

THE EFFECTS OF WARPING CONSTRAINTS ON THE BUCKLING OF THIN-WALLED STRUCTURES

MARCELLO PIGNATARO, NICOLA RIZZI, GIUSEPPE RUTA AND VALERIO VARANO

We present two applications of a direct one-dimensional beam model suitable for describing the buckling of thin-walled structures. The first application considers the buckling of a compressed beam with an intermediate stiffener under various warping constraints. The second describes the buckling of a two-bar frame, known as a Roorda frame, loaded by a dead force at the joint. Various warping constraints at the bar ends are considered and the relevant buckling modes and loads are numerically evaluated. Numerical results are presented for both cases; some of these appear to be new.

1. Introduction: a direct one-dimensional model for thin-walled beams

A very interesting problem in the elastic stability of structural elements is the flexural-torsional buckling of thin-walled beams. A short description of the origins of the problem with references to related existing literature may be found in [Ruta et al. 2006; 2008].

In [Ruta et al. 2006] the direct model introduced in [Tatone and Rizzi 1991; Rizzi and Tatone 1996] was refined in order to describe the flexural-torsional buckling of beams with nonsymmetric cross-sections. Strain measures are described with respect to both the centroidal and the shear center axes of the beam (as a first step, it is immaterial which of the shear centers presented in the literature is chosen). The power expended by inner actions is decomposed so as to distinguish between forces and moments at the centroid or the shear center. Nonlinear hyperelastic constitutive relations and standard inner constraints [Rizzi and Tatone 1996; Pignataro and Ruta 2003; Pignataro et al. 2006] imply reactive terms in addition to the active parts of some contact actions, accounting for the geometry of nonsymmetric cross-sections. The obtained field equations for the bifurcation in terms of the displacement components are more general than those in [Rizzi and Tatone 1996; Pignataro and Ruta 2003; Pignataro et al. 2006].

In [Ruta et al. 2006] some simple examples of flexural-torsional buckling and postbuckling phenomena have been investigated, showing the coincidence of the results with those in the literature, for instance in [Timoshenko and Gere 1961; Grimaldi and Pignataro 1979]. Further applications of the refined model are found in [Ruta et al. 2008] where, for a simply supported compressed beam, the effect of warping constraints at the beam ends has been examined and the relevant critical loads have been presented.

A natural development of the studies performed in [Ruta et al. 2006; 2008] appears to be the analysis of the buckling of more complex structures by means of the refined model. In this paper, the authors present two cases of interest in applications. The first is a compressed beam reinforced by an intermediate stiffener acting as a warping constraint. The second is a simple frame loaded by a dead force, known

Keywords: thin-walled structures, flexural-torsional buckling, warping constraints.

M. Pignataro and G. Ruta gratefully acknowledge the partial support of the grant *Ricerche di Università* of the University of Rome 'La Sapienza' for the year 2008.

as a Roorda frame in the literature. We first summarize the key notes of the refined model (details are found in [Ruta et al. 2006; 2008]); then, we present the field equations for the considered problems and some numerical results.

The beam reference shape consists of a series of plane cross-sections orthogonally attached to the straight centroidal axis, or to the parallel shear center axis. We fix orthogonal cartesian coordinates with x_1 parallel to the beam axes and a consistent orthonormal right-handed vector basis $(\mathbf{i}_1, \mathbf{i}_2, \mathbf{i}_3)$. Suitable strain measures are

$$\begin{aligned} \mathbf{E} &= \mathbf{R}^\top \mathbf{R}' = \chi_1 \mathbf{i}_2 \wedge \mathbf{i}_3 + \chi_2 \mathbf{i}_3 \wedge \mathbf{i}_1 + \chi_3 \mathbf{i}_1 \wedge \mathbf{i}_2, \\ \mathbf{e}_o &= \mathbf{R}^\top \mathbf{p}'_o - \mathbf{q}'_o = \varepsilon_1 \mathbf{i}_1 + \varepsilon_2 \mathbf{i}_2 + \varepsilon_3 \mathbf{i}_3, \\ \mathbf{e}_c &= \mathbf{R}^\top \mathbf{p}'_c - \mathbf{q}'_c = \mathbf{e}_o + \mathbf{E} \mathbf{c} = \varepsilon_{1c} \mathbf{i}_1 + \varepsilon_{2c} \mathbf{i}_2 + \varepsilon_{3c} \mathbf{i}_3 \\ &= (\varepsilon_1 + \chi_2 c_3 - \chi_3 c_2) \mathbf{i}_1 + (\varepsilon_2 - \chi_1 c_3) \mathbf{i}_2 + (\varepsilon_3 + \chi_1 c_2) \mathbf{i}_3, \quad \alpha, \quad \eta = \alpha', \end{aligned} \quad (1-1)$$

where o is the centroid, c is the shear center, and $\mathbf{c} = c_2 \mathbf{i}_2 + c_3 \mathbf{i}_3 = c - o$; $\mathbf{p}_o(x_1, t)$ and $\mathbf{p}_c(x_1, t)$ are the vector-valued present placements of the axes, given by $\mathbf{q}_o(x_1)$ and $\mathbf{q}_c(x_1)$ in the reference shape; $\mathbf{R}(x_1, t)$ is the proper orthogonal tensor-valued cross-sectional rotation from the reference to the present shape; and $\alpha(x_1, t)$ is the scalar-valued coarse descriptor of warping. The skew tensor \mathbf{E} provides the curvature of the beam axes, and the vectors \mathbf{e}_o and \mathbf{e}_c measure the differences between the tangent to the axes in the present and reference shape. We have defined χ_1 as the torsion curvature (twist); χ_2 and χ_3 as the bending curvatures; the wedge product \wedge between vectors provides skew tensors; ε_1 is the elongation of the centroidal axis; and ε_2 and ε_3 are the shearing strains between this axis and the cross-sections. We decompose the displacement of the centroidal axis and the rotation:

$$\mathbf{u} = \mathbf{p}_o - \mathbf{q}_o = u_1 \mathbf{i}_1 + u_2 \mathbf{i}_2 + u_3 \mathbf{i}_3, \quad \mathbf{R} = \mathbf{R}_3 \mathbf{R}_2 \mathbf{R}_1, \quad (1-2)$$

where \mathbf{R}_1 is a rotation of amplitude φ_1 around \mathbf{i}_1 ; \mathbf{R}_2 is a rotation of amplitude φ_2 around $\mathbf{R}_1 \mathbf{i}_2$; \mathbf{R}_3 is a rotation of amplitude φ_3 around $\mathbf{R}_2 \mathbf{R}_1 \mathbf{i}_3$.

The power P^e expended by external actions is a linear functional of the velocities with respect to the shear center, while the power P^i expended by the interactions among different parts of the beam is a linear functional of the velocities with respect to the shear center and of their first derivatives with respect to x_1 (grade one theory, see, for example, [DiCarlo 1996]). Standard arguments on the balance of power and a pull-back procedure [Ruta et al. 2006; 2008] yield the local balance of force and torque in the reference shape with respect to c , the auxiliary equations for bishear and bimoment and the internal power:

$$\begin{aligned} \mathbf{s}' + \mathbf{E} \mathbf{s} + \mathbf{a} &= \mathbf{0}, \quad \mathbf{S}' + \mathbf{E} \mathbf{S} - \mathbf{S} \mathbf{E} + (\mathbf{q}'_c + \mathbf{e}_c) \wedge \mathbf{s} + \mathbf{A} = \mathbf{0}, \\ \tau &= \beta + \mu', \quad P^i = \int_0^l (\mathbf{s} \cdot \dot{\mathbf{e}}_c + \mathbf{S} \cdot \dot{\mathbf{E}} + \tau \omega + \mu \omega'). \end{aligned} \quad (1-3)$$

The vectors \mathbf{a} and \mathbf{s} are the bulk and contact forces; the skew tensors \mathbf{A} and \mathbf{S} are the bulk and contact couples; the scalar β is the bulk action spending power on warping; the scalars μ and τ are the bimoment and bishear [Vlasov 1961], respectively, all in the reference shape. We pose:

$$\mathbf{s} = Q_1 \mathbf{i}_1 + Q_2 \mathbf{i}_2 + Q_3 \mathbf{i}_3, \quad \mathbf{S} = S_1 \mathbf{i}_2 \wedge \mathbf{i}_3 + S_2 \mathbf{i}_3 \wedge \mathbf{i}_1 + S_3 \mathbf{i}_1 \wedge \mathbf{i}_2. \quad (1-4)$$

By introducing equations (1-1) and (1-4) into (1-3)₄, the internal power reads

$$\int_0^l [Q_1 \dot{\varepsilon}_1 + Q_2 \dot{\varepsilon}_{2c} + Q_3 \dot{\varepsilon}_{3c} + S_1 \dot{\chi}_1 + (S_2 + c_3 Q_1) \dot{\chi}_2 + (S_3 - c_2 Q_1) \dot{\chi}_3 + \tau \omega + \mu \omega'], \quad (1-5)$$

that is, the normal force Q_1 spends power on the centroidal straining, while the shearing forces Q_2 and Q_3 are applied at the shear center; S_1 is the twisting couple, while $M_2 = S_2 + c_3 Q_1$ and $M_3 = S_3 - c_2 Q_1$ are the bending torques, evaluated with respect to the centroid.

If ζ is a constant, we postulate the inner constraints [Vlasov 1961; Reissner 1983; Simo and Vu-Quoc 1991; Tatone and Rizzi 1991; Rizzi and Tatone 1996]

$$\alpha = \zeta \chi_1, \quad \zeta \in \mathbb{R}, \quad \eta = \zeta \chi_1', \quad \mathbf{e}_o = \varepsilon_1 \mathbf{q}'_o = \varepsilon_1 \mathbf{e}_1, \quad \varepsilon_2 = \varepsilon_3 = 0. \quad (1-6)$$

The cross-sections and shear axis do not remain normal ($\varepsilon_{2c} \neq 0$, $\varepsilon_{3c} \neq 0$; see (1-1)).

If the beam is homogeneous and elastic, the material response depends on \mathbf{e} , \mathbf{E} , α , and η and inner constraints make the contact actions consist of an active and a reactive part [Truesdell and Noll 1965]. The former (subscript a) is determined by a constitutive relation; the latter (subscript r) spends no power on the velocities compatible with the constraints [Truesdell and Noll 1965]. In our refined model, the normal force, the bending torques, and the bimoment are entirely active, while the shearing forces and the bishear have a reactive part [Ruta et al. 2006; 2008]; the reactive twisting torque S_{1r} contains the bishear, in accord with the literature [Vlasov 1961]. As is customary, we suppose that the shearing force and the bishear depend only on the shearing strain, which makes them purely constraint reactions. Thus, some actions are entirely active, others reactive, and only the twisting torque has both components [Ruta et al. 2006; 2008].

We adopt nonlinear hyperelastic constitutive relations in order to apply Koiter's theory [1945] and a static perturbation technique [Budiansky 1974]:

$$\begin{aligned} Q_{1a} = Q_1 &= a \varepsilon_1 + \frac{1}{2} d \chi_1^2, & S_{1a} &= (k + d \varepsilon_1 + f_2 \chi_2 + f_3 \chi_3 + g \eta) \chi_1, \\ M_{2a} = M_2 &= b_2 \chi_2 + \frac{1}{2} f_2 \chi_1^2, & M_{3a} = M_3 &= b_3 \chi_3 + \frac{1}{2} f_3 \chi_1^2, & \mu_a = \mu &= h \eta + \frac{1}{2} g \chi_1^2. \end{aligned} \quad (1-7)$$

The coefficients a , b_j ($j = 2, 3$), k , and h are the rigidities in extension, bending, torsion, and warping, respectively; d , f_j ($j = 2, 3$), and g take into account the couplings between extension and torsion, bending and torsion, and warping and torsion, respectively [Truesdell and Noll 1965; Møllmann 1986]. If, as is standard, the bulk action β vanishes, we obtain [Ruta et al. 2006; 2008]

$$\tau = h \zeta \chi_1'' + g \chi_1 \chi_1', \quad S_1 = (k + d \varepsilon_1 + f_2 \chi_2 + f_3 \chi_3) \chi_1 - h \zeta^2 \chi_1'' + c_3 Q_2 - c_2 Q_3. \quad (1-8)$$

Comparing [Vlasov 1961, equation (V.1.10)₃] with ours we obtain

$$\begin{aligned} a &= EA, & b_j &= EI_j \quad (j = 2, 3), & k &= GI_c, \\ d &= EI_d, & f_j &= EI_{f_j} \quad (j = 2, 3), & h \zeta^2 &= EI_\omega; \end{aligned} \quad (1-9)$$

E and G are the moduli in extension and shear; A is the cross-sectional area; I_j ($j = 2, 3$) are the centroidal principal moments of inertia; I_c is the torsion factor; I_d is the polar inertia with respect to c ; I_ω is the warping inertia (second moment of the sectorial coordinate with respect to the area); $I_{f_2} = \int_A x_3 r^2$; and $I_{f_3} = \int_A x_2 r^2$, with x_j ($j = 2, 3$) the coordinates of a point with respect to the centroid and r its distance from the shear center.

2. Buckling of a compressed beam with a warping stiffener

For a beam compressed by a dead centroidal load of magnitude λ , one solution of the elastic static problem, called the *fundamental* path and denoted by the superscript f, is:

$$\begin{aligned} \mathbf{u}^f &= -\frac{\lambda}{a}x_1\mathbf{i}_1, & \mathbf{R}^f &= \mathbf{I}, & \alpha^f &= 0, \\ \mathbf{e}^f &= -\frac{\lambda}{a}\mathbf{i}_1, & \mathbf{E}^f &= \mathbf{0}, & \eta^f &= 0, \\ \mathbf{s}^f &= -\lambda\mathbf{i}_1, & \mathbf{S}^f &= \mathbf{0}, & \tau^f &= 0, & \mu^f &= 0. \end{aligned} \quad (2-1)$$

A different solution, called the *bifurcated* path and denoted by the superscript b, is

$$\begin{aligned} \mathbf{u}^b &= \mathbf{u} - \frac{\lambda}{a}x_1\mathbf{i}_1, & \mathbf{R}^b &= \mathbf{R} + \mathbf{I}, & \alpha^b &= \alpha, \\ \mathbf{e}^b &= \mathbf{e} - \frac{\lambda}{a}\mathbf{i}_1, & \mathbf{E}^b &= \mathbf{E}, & \eta^b &= \eta, \\ \mathbf{s}^b &= \mathbf{s} - \lambda\mathbf{i}_1, & \mathbf{S}^b &= \mathbf{S}, & \tau^b &= \tau, & \mu^b &= \mu. \end{aligned} \quad (2-2)$$

The differences of quantities evaluated along the bifurcated and the fundamental paths are expressed without superscripts, that is, $(\cdot) := (\cdot)^b - (\cdot)^f$. Strain measures, balance, and auxiliary equations, as well as constitutive relations, are written in terms of differences. The latter are supposed to regularly depend on a parameter σ :

$$(\cdot) = (\cdot)(\sigma), \quad \sigma \in [0, 1], \quad (\cdot)|_{\sigma=0} = 0. \quad (2-3)$$

A formal σ -power series expansion of the quantities of interest in a neighborhood of $\sigma = 0$ provides the first-order equations of interest for the buckling,

$$\begin{aligned} \bar{u}_1'' = 0, \quad b_3\bar{u}_2'''' + \lambda\frac{a-\lambda}{a}(\bar{u}_2'' - c_3\bar{\varphi}_1'') = 0, \quad b_2\bar{u}_3'''' + \lambda\frac{a-\lambda}{a}(\bar{u}_3'' + c_2\bar{\varphi}_1'') = 0, \\ h\zeta^2\bar{\varphi}_1'''' + \frac{d\lambda - ak}{a}\bar{\varphi}_1'' + \lambda\frac{a}{a-\lambda}(c_2\bar{u}_3'' - c_3\bar{u}_2'') = 0, \end{aligned} \quad (2-4)$$

with the overbar standing for increments of first order in σ .

We have considered the case of a beam with an intermediate stiffener, preventing warping in a section $x_1 = m$, $m \in (0, l)$. A number of values of m and of the boundary conditions have been considered. Each problem has been solved numerically using the COMSOL Multiphysics FEM code, available at the Dipartimento di Strutture of the Università Roma Tre. For this purpose, (2-4) has been written in weak form on the two regular subdomains $x_1 \in (0, m)$ and $x_1 \in (m, l)$. Then, giving the appropriate boundary conditions, the eigenvalue problems providing the critical values λ_c of the load multiplier and the mode shapes \bar{u}_{2c} , \bar{u}_{3c} , and $\bar{\varphi}_{1c}$, have been solved using the COMSOL PDE application.

Consider a beam channel with length $l = 2000$ mm, outer dimensions 100 mm (web), 60 mm (flanges), and uniform thickness of 3 mm [Ruta et al. 2008]. Let the x_3 -axis of the chosen cartesian system coincide with the symmetry axis of the cross-section. The geometric and inertial quantities have been derived by means of standard calculations and well-known tables, such as those in [Timoshenko and Gere 1961]. Let the material of the beam be elastic and isotropic and characterized by $E = 206$ GPa, $G = 79$ GPa.

The constitutive coefficients (1-9) are

$$\begin{aligned}
 a = 642 \text{ mm}^2 E, \quad b_3 = 1054726 \text{ mm}^4 E, \quad h\xi^2 = 446086956 \text{ mm}^6 E, \quad k = 1875 \text{ mm}^4 G, \\
 d = 2370581 \text{ mm}^4 E, \quad b_2 = 236653 \text{ mm}^4 E, \quad c_3 = -41 \text{ mm}, \quad c_2 = 0 \text{ mm}.
 \end{aligned}
 \tag{2-5}$$

We assume that the beam is simply supported, with torsional rotation prevented at both ends. The corresponding boundary conditions in terms of first-order quantities are

$$\bar{\varphi}_1 = \bar{u}_2 = \bar{u}_3 = \bar{u}_2'' = \bar{u}_3'' = 0, \quad \text{in } x_1 = 0, \quad x_1 = l.
 \tag{2-6}$$

Continuity conditions must be imposed in the section $x_1 = m$, where the stiffener is present. We will consider the following three cases:

- (1) warping is free in both $x_1 = 0$ and $x_1 = l$;
- (2) warping is prevented in $x_1 = 0$ and free in $x_1 = l$;
- (3) warping is prevented in both $x_1 = 0$ and $x_1 = l$.

For each case, we study how the buckling is affected when the warping is prevented by the stiffener. Then, in addition to the continuity conditions, the warping constraint at $x_1 = m$ must be taken into account. In the following, we present the critical loads and the corresponding buckling modes. For the sake of simplicity, overbars and subscript c are omitted.

Figure 1 shows the flexural-torsional critical mode associated with boundary condition (1) and with the stiffener located at $m = 400 \text{ mm}$. The first plot in the figure shows the flexural component of the buckling mode, while the second graph illustrates the torsional component. It is apparent, as it was to be expected, that the flexural mode is exactly the same as in Euler buckling (a half sine wave), while the torsional component has a stationary point by correspondence with the stiffener (where $\alpha = \varphi_1' = 0$).

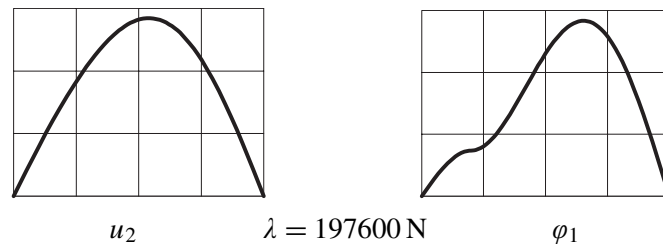


Figure 1. Beam warping-free at the ends, with stiffener at $m = 400 \text{ mm}$.

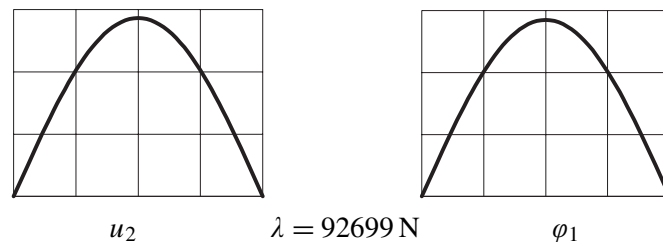


Figure 2. Beam warping-free at the ends, without stiffener.

This mode is compared with that for the beam without the stiffener, shown in Figure 2, where the corresponding critical load is also indicated. The difference, as was to be expected, is in the torsional component which in absence of the stiffener remains a half sine wave. Moreover, the critical load is significantly lower than the previous one.

In Figure 3 the flexural-torsional critical mode associated with case (2) and with the stiffener located at $m = 1600$ mm is shown. The first plot shows the flexural component of the buckling mode, while the second graph illustrates the torsional component. It is apparent, as expected, that the flexural component corresponds to Euler buckling (a half sine wave) while the torsional component has a stationary point by correspondence with the stiffener (where $\alpha = \varphi_1' = 0$). Notice also that the restrained warping at one end (for instance, $x_1 = 0$ in this case) is represented by a horizontal tangent in the graph for the torsional component, φ_1 , of the buckling mode. The critical load is significantly higher than that shown in Figure 1, confirming that the system is globally stiffer.

The two components of this buckled shape are compared with the corresponding ones for the beam without a stiffener shown in Figure 4. Here it emerges that the two components of the mixed buckling mode are still a half-sine wave for the flexural part and a curve with initial zero slope, due to the restrained warping at the origin, for the torsional part. The critical load is significantly lower than the previous one.

In Figure 5 the flexural-torsional critical mode associated with case (3) and with the stiffener located at $m = 400$ mm is shown. The first plot shows the flexural component of the buckling mode, and the second graph illustrates the torsional component. Once again, as was to be expected, the flexural mode corresponds to Euler buckling (a half sine wave) since it remains unaltered by the constraints on the torsional rotation and on the warping. The torsional component has a stationary point by correspondence with the stiffener (where $\alpha = \varphi_1' = 0$) and the restrained warping at both ends is represented by horizontal tangents in the graph for the torsional component φ_1 of the buckling mode. The critical load attains the maximum value among those seen so far.

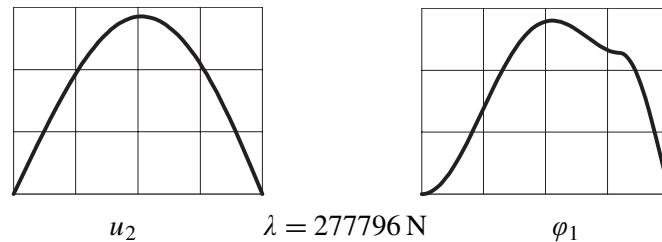


Figure 3. Beam with warping restrained at one end and stiffener at $m = 1600$ mm.

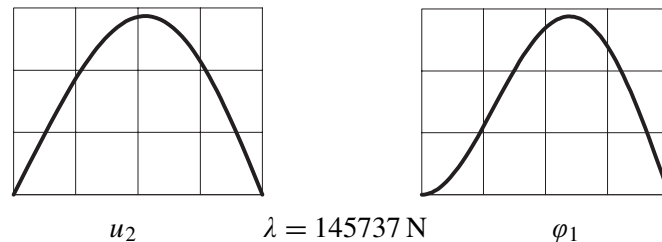


Figure 4. Beam with warping restrained at one end, without stiffener.

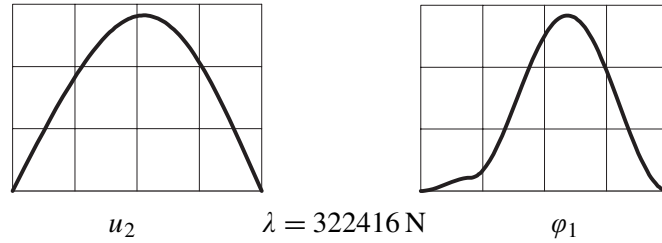


Figure 5. Beam with warping restrained at both ends and stiffener at $m = 400$ mm.

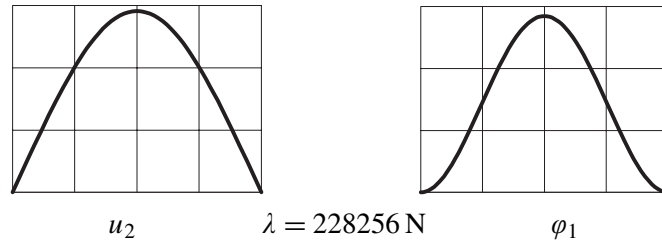


Figure 6. Beam with warping restrained at both ends, without stiffener.

The components of the mixed buckling are compared with the corresponding ones for the beam without a stiffener, shown in Figure 6, where it turns out that the mixed buckling in the absence of the stiffener is composed of two modes symmetric with respect to the midspan. The transverse displacement is a half sine wave, while the horizontal tangents at the ends of the torsional rotation point out the presence of the warping constraints.

Figure 7 shows the values of the critical load versus the position of the stiffener. The horizontal line shows the value of the Euler critical load, which is not affected by the warping restrictions at the beam ends and at the stiffener, when flexural buckling occurs around the axis of smaller inertia (x_2 for the cross-section considered). The other curves show the values of the critical load for flexural-torsional buckling.

We note that when a stiffener is located at $m = \frac{1}{2}$ and the boundary conditions are those of case (1), the Euler buckling load around the axis of smaller inertia is higher than the flexural-torsional one.

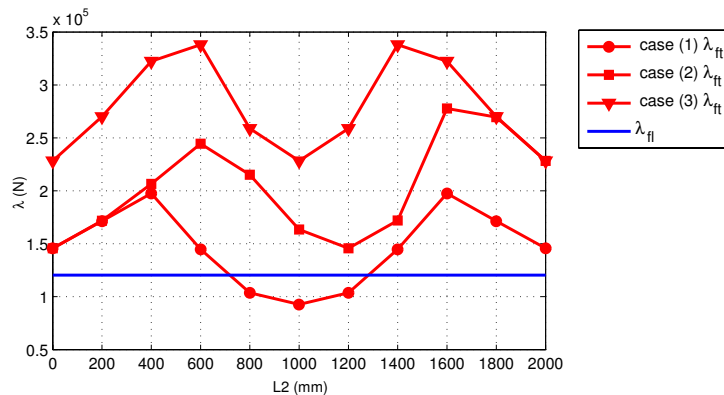


Figure 7. Numerical results.

This happens also when both ends are free to warp and no stiffener is present, as shown in [Ruta et al. 2008]. In fact, due to the symmetry of the torsional rotation (see Figure 2) the warping vanishes at midspan. By inserting a stiffener in a different section the flexural-torsional critical load in general varies nonmonotonically.

With reference to Figure 7, when both ends are free to warp, as in case (1), for $m \in [0, 700)$ or $m \in (1300, 2000]$ the flexural-torsional critical load is higher than the Euler one while for $m \in (700, 1300)$ the opposite happens (all lengths are here expressed in millimeters). The maximum value of the critical load is attained at $m = 400$ or $m = 1600$, since the dependence of the flexural-torsional critical load on the location of the stiffener is in this case symmetric with respect to the midspan. On the other hand, as it was already pointed out, the symmetry of both the components of the mixed buckling mode fails, see Figure 1.

When warping is prevented at both ends, case (3), the flexural-torsional critical load is higher than the Euler buckling load in the plane of smaller inertia, irrespective of the stiffener location. This is of importance in applications, since in practice design against buckling could be restricted to Euler buckling in the plane of smaller inertia simply by preventing warping at the ends and inserting an intermediate stiffener at will. The maximum effect of the increase of the critical load, however, is attained when the stiffener is located at $m = 600$ or $m = 1400$. Indeed, here also the dependence of the flexural-torsional critical load on the location of the stiffener is symmetric with respect to the midspan.

If warping is restrained at one end, described by case (2), the curve representing the effect of the intermediate stiffener coincides at $m = 0$ with the curve representing case (1). By increasing m , the flexural-torsional critical load increases in a nonmonotonic way, and the curve tends to the one representing case (3). In particular, the two curves coincide at $m = 2000$. In this case, as well as in the previous one, the entire curve lies above the straight horizontal line representing the Euler buckling load in the plane of smaller inertia. This is again of some importance in applications.

It must be stressed that the curves in the preceding figures change dramatically if the beam length is changed, fixing all the other parameters. In particular, as shown in [Ruta et al. 2008], the flexural-torsional critical load for case (1) coincides with the Euler one in the plane of smaller inertia when $l = 2731$ mm. It may be shown that when $l > 2731$ mm the curves describing the dependence of the flexural-torsional critical load on the stiffener location always lie above the straight horizontal line representing the Euler buckling load in the plane of smaller inertia, irrespective of the stiffener location.

3. Bifurcations in a two-bar frame

We now consider a two-bar frame, called a Roorda frame in the literature on stability of structures [Bažant and Cedolin 1991] and exhibiting interesting interactions between flexural and torsional modes occurring out of the frame plane. Results for the buckling of a frame made of I-beams are in [Pignataro et al. 2006]: two buckling modes are possible, one in-plane flexural (Euler-like) and another flexural-torsional, where one of the bars undergoes torsion while the other bends out of the plane. These results are of limited applicability, since the beam model in [Pignataro et al. 2006] cannot describe thin-walled elements with generic cross-sections as pointed out in Section 1.

It is thus interesting to study the buckling of a Roorda frame composed of thin-walled beams with nonsymmetric cross-sections, which are widely used in many structures (a standard example being the

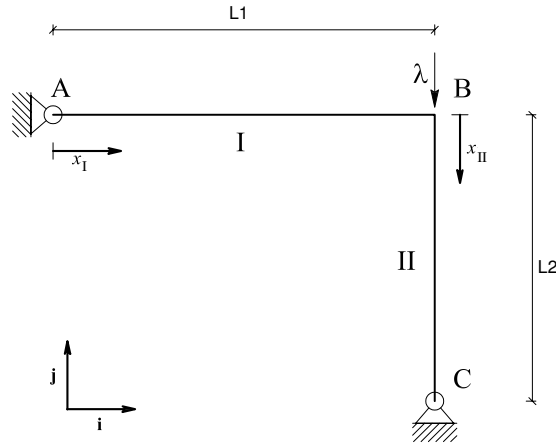


Figure 8. Two-bar frame.

so-called rack structures). In the literature there are numerical results obtained via refined finite element codes and experimental studies on the subject. Some of these, regarding a frame shaped spatial beam, are in [Kim and Kim 2000; Kim et al. 2001; Gu and Chan 2005; Teh 2005]. Still, to the authors’ knowledge, an analytical study derived from a geometrically exact model is not available and the results obtained here could be of importance in applications.

Despite the fact that the model in [Ruta et al. 2006; 2008] considers generic cross-sections, we limit our study to a frame with beams exhibiting one axis of symmetry. This does not limit the generality of the results for two reasons: on one hand, the coupling between flexural and torsional buckling, so important in these structures, is clearly put into evidence; on the other hand, beams with one axis of symmetry such as channels are of widespread use.

Consider the frame in Figure 8: the bars AB (the beam) and BC (the column) are hinged to the ground in A and C and clamped at the common joint B. The frame is loaded at B by a dead load of magnitude λ in order to apply standard techniques [Koiter 1945; Budiansky 1974]. A global basis and local abscissas are indicated in the figure; the subscripts I and II distinguish quantities referring to the beam and the column, respectively. We take into account the possibility of various warping constraints at the beam ends A, B, and C.

The fundamental equilibrium path is

$$\begin{aligned}
 \mathbf{u}_I^f &= \mathbf{0}, & \mathbf{R}_I^f &= \mathbf{I}, & \alpha_I^f &= 0, \\
 \mathbf{e}_I^f &= \mathbf{0}, & \mathbf{E}_I^f &= \mathbf{0}, & \eta_I^f &= 0, \\
 \mathbf{s}_I^f &= \mathbf{0}, & \mathbf{S}_I^f &= \mathbf{0}, & \tau_I^f &= 0, & \mu_I^f &= 0, \\
 \mathbf{u}_{II}^f &= -\frac{\lambda}{a} x_{II} \mathbf{i}_1, & \mathbf{R}_{II}^f &= \mathbf{I}, & \alpha_{II}^f &= 0, \\
 \mathbf{e}_{II}^f &= -\frac{\lambda}{a} \mathbf{i}_1, & \mathbf{E}_{II}^f &= \mathbf{0}, & \eta_{II}^f &= 0, \\
 \mathbf{s}_{II}^f &= -\lambda \mathbf{i}_1, & \mathbf{S}_{II}^f &= \mathbf{0}, & \tau_{II}^f &= 0, & \mu_{II}^f &= 0.
 \end{aligned} \tag{3-1}$$

The bifurcated path is written in terms of the differences

$$\begin{aligned}
 \mathbf{u}_I^b &= \mathbf{u}, & \mathbf{R}_I^b &= \mathbf{R} + \mathbf{I}, & \alpha_I^b &= \alpha, \\
 \mathbf{e}_I^b &= \mathbf{e}, & \mathbf{E}_I^b &= \mathbf{E}, & \eta_I^b &= \eta, \\
 \mathbf{s}_I^b &= \mathbf{s}, & \mathbf{S}_I^b &= \mathbf{S}, & \tau_I^b &= \tau, & \mu_I^b &= \mu, \\
 \mathbf{u}_{II}^b &= \mathbf{u} - \frac{\lambda}{a} x_1 \mathbf{i}_1, & \mathbf{R}_{II}^b &= \mathbf{R} + \mathbf{I}, & \alpha_{II}^b &= \alpha, \\
 \mathbf{e}_{II}^b &= \mathbf{e} - \frac{\lambda}{a} \mathbf{i}_1, & \mathbf{E}_{II}^b &= \mathbf{E}, & \eta_{II}^b &= \eta, \\
 \mathbf{s}_{II}^b &= \mathbf{s} - \lambda \mathbf{i}_1, & \mathbf{S}_{II}^b &= \mathbf{S}, & \tau_{II}^b &= \tau, & \mu_{II}^b &= \mu.
 \end{aligned} \tag{3-2}$$

Operating as in Section 2, some steps provide the first-order equations for the buckling in terms of the displacement components

$$\left. \begin{aligned}
 \bar{u}_1'' &= 0, & b_3 \bar{u}_2'''' &= 0, & b_2 \bar{u}_3'''' &= 0, & h \xi^2 \bar{\varphi}_1'''' - k \bar{\varphi}_1'' &= 0 & \text{on AB,} \\
 \bar{u}_1'' &= 0, & b_3 \bar{u}_2'''' + \lambda \frac{a-\lambda}{a} (\bar{u}_2'' - c_3 \bar{\varphi}_1'') &= 0, & b_2 \bar{u}_3'''' + \lambda \frac{a-\lambda}{a} (\bar{u}_3'' + c_2 \bar{\varphi}_1'') &= 0, \\
 h \xi^2 \bar{\varphi}_1'''' + \frac{d\lambda - ak}{a} \bar{\varphi}_1'' + \lambda \frac{a}{a-\lambda} (c_2 \bar{u}_3'' - c_3 \bar{u}_2'') &= 0 & & & & & & \text{on BC.}
 \end{aligned} \right\} \tag{3-3}$$

Equations (3-3) plus boundary conditions constitute an eigenvalue problem providing the critical values λ_c and the mode shapes \bar{u}_{2c} , \bar{u}_{3c} , and $\bar{\varphi}_{1c}$. For simplicity of notation, the overbars indicating first-order quantities have been dropped in the following, as has subscript c . The effect of different warping constraints at the ends of the beams composing the frame on the critical loads has been studied numerically by means of the COMSOL code.

3A. Geometrical and material data. Two benchmark cases have been considered, characterized by two different cross sections exhibiting two and one axes of symmetry, respectively: a wide flange HEA240 and a channel (U-shape) with outer dimensions 100 mm (web) and 60 mm (flanges) and a uniform thickness of 3 mm. By assuming the local coordinate systems as in Figure 9, the geometric and inertial quantities of the cross-section are obtained by standard calculations and well-known tables [Timoshenko and Gere 1961; Pignataro et al. 1991]:

- U100:

$$\begin{aligned}
 a &= 642 \text{ mm}^2 E, & b_3 &= 1054726 \text{ mm}^4 E, & h \xi^2 &= 446086956 \text{ mm}^6 E, & k &= 1875 \text{ mm}^4 G, \\
 d &= 2370581 \text{ mm}^4 E, & b_2 &= 236653 \text{ mm}^4 E, & c_3 &= -41 \text{ mm}, & c_2 &= 0 \text{ mm};
 \end{aligned}$$

- HEA240:

$$\begin{aligned}
 a &= 7.68 \times 10^3 \text{ mm}^2 E, & b_2 &= 2.769 \times 10^7 \text{ mm}^4 E, & h \xi^2 &= 3.65 \times 10^{11} \text{ mm}^6 E, \\
 k &= 3.1 \times 10^5 \text{ mm}^4 G, & d &= 1.05 \times 10^8 \text{ mm}^4 E, & b_3 &= 7.763 \times 10^7 \text{ mm}^4 E, & c_3 &= c_2 = 0 \text{ mm}.
 \end{aligned}$$

We assume the Young's modulus is $E = 206$ GPa and the shear modulus $G = 79$ GPa as in Section 2.

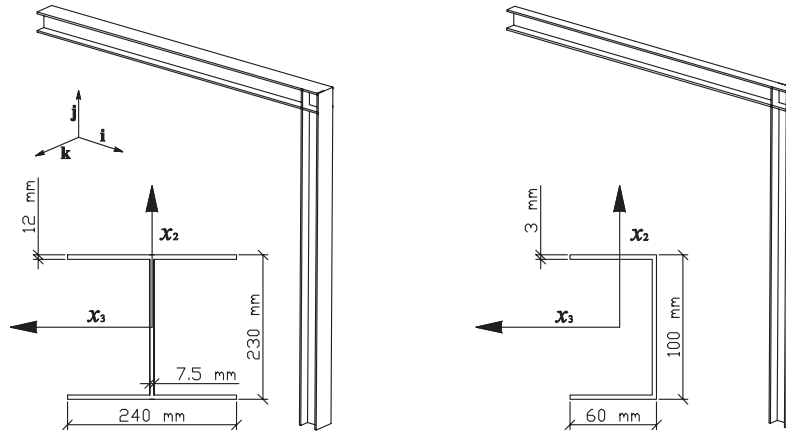


Figure 9. Three-dimensional view.

3B. Boundary conditions. In [Pignataro et al. 2006] a two-bar frame such as that in Figure 8 was analyzed. At the ends A and C the rotations φ_2 and φ_3 were assumed to be free while it was supposed $\varphi_1 = 0$. In addition, the joint B was allowed to move out of the plane of the frame: this resulted in a very low critical load. This case, however, is hardly of any technical interest due to the fact that in 3D frames actual hinges are cylindrical and the out-of-plane movement of nodes like B is controlled by the presence of braces.

In this section, therefore, we consider the case in which node B is prevented from moving along the unit vector k and the hinges in A and C allow the sole rotation along k . This results in the following boundary conditions:

$$\begin{aligned}
 & \mathbf{u} = \mathbf{0}, \quad \varphi_1 = 0, \quad \varphi_2 = 0, \quad M_3 = 0, & \text{in A and C;} \\
 & \mathbf{u}_I = \mathbf{u}_{II}, \quad \mathbf{R}_I = \mathbf{R}_{II}, \quad \mathbf{S}_I = \mathbf{S}_{II}, \quad \mathbf{u}_I \cdot \mathbf{k} = 0, \quad (\mathbf{I} - \mathbf{k} \otimes \mathbf{k})(s_I - s_{II}) = \mathbf{0}, & \text{in B.}
 \end{aligned}$$

In order to investigate the influence of warping on buckling, some additional boundary conditions on the warping are assumed, as follows:

case	node A	node B	node C
a	free	free	free
b	free	prevented	free
c	prevented	free	prevented
d	prevented	prevented	prevented

Here “prevented” stands for warping prevented and “free” stands for no constraint on warping which implies vanishing bimoment at the indicated beam ends. Details of the boundary conditions at node B are shown in Figure 10.

This results in four cases:

- Case a: $\mu = 0$ in A, B and C;
- Case b: $\mu = 0$ in A and C, and $\alpha = 0$ in B;
- Case c: $\mu = 0$ in B, and $\alpha = 0$ in A and C;
- Case d: $\alpha = 0$ in A, B and C.

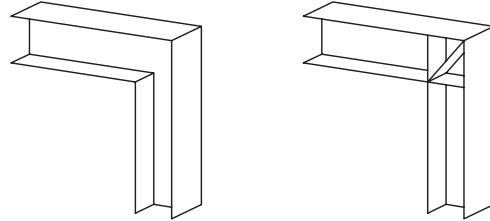


Figure 10. Detail of frame joint B, warping free (left) and warping restrained (right).

3C. Numerical examples. In this section we consider a set of frames in which the length of the beam (say L_1) is fixed to 2000 mm, while the length of the column (say L_2) has been varied in the range 3000 mm–8000 mm.

Results have been obtained for each of the boundary cases a–d.

3C.1. Modes. Figures 11 and 12 refer to the frame with HEA240 beams and show the buckling modes and the corresponding critical value of the load multiplier. It is apparent that the considered frame may buckle in three different ways:

Mode 1 is purely flexural (Euler-like) in the plane of the frame and involves both beam and column (see Figure 11, mode u_2);

Mode 2 is purely torsional and involves the sole column (see Figure 11, mode φ_1) which buckles in the shape of a half-sine wave while the beam remains straight;

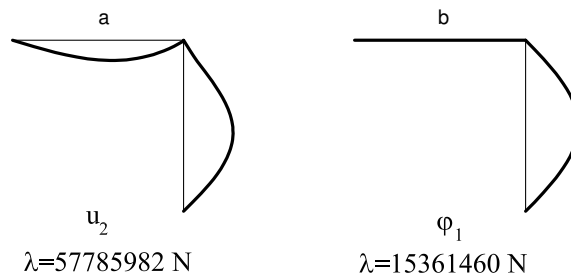


Figure 11. HEA240: In-plane flexural mode and torsional mode.

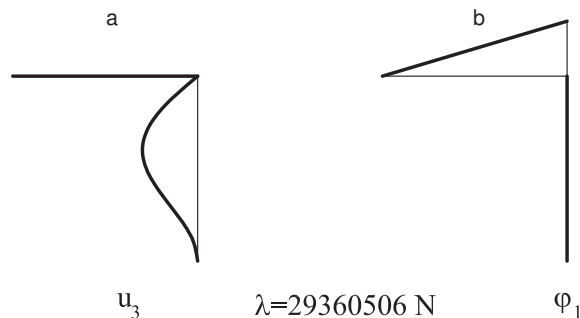


Figure 12. HEA240: Out-of-plane flexural mode.

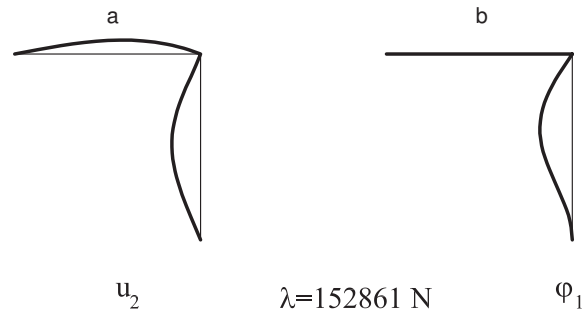


Figure 13. U100 flexural-torsional mode.

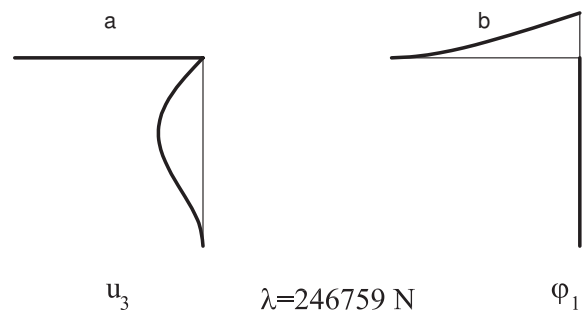


Figure 14. U100 flexural mode out of plane.

Mode 3 is such that the column bends out of the plane of the frame while the beam twists, acting only as a flexural constraint in B (see Figure 12). On the other hand, the torsional rotation is different from zero only in the beam where it has the linear behavior characteristic of the Saint-Venant uniform torsion.

This result, apart from the different constraint on the out-of-plane displacement of the joint B, corresponds to that in [Pignataro et al. 2006]: when the centroid coincides with the shear center of the cross-sections no coupling exists between the buckling modes which are either flexural or torsional and may be different for the two bars simply for geometrical reasons (in section B a torsional rotation of the beam is a bending rotation of the column).

When the frame bars have cross-sections with one symmetry axis only the frame may buckle in two ways only as shown in Figures 13 and 14:

Mode 4 is such that the beam is subjected only to flexure in the plane of the frame, while the column undergoes flexure and torsion (see Figure 13). Note that the torsional mode has zero initial slope due to the warping constraint in C;

the other mode (see Figure 14) corresponds to the buckling mode 3 before except for the initial zero slope of the torsional mode due to the warping constraint.

3C.2. Critical loads. Figures 15 and 16 show the values of the critical load (expressed in N) versus the length L_2 of the column for each of the warping constraints in cases a–d for the HEA240 and U100

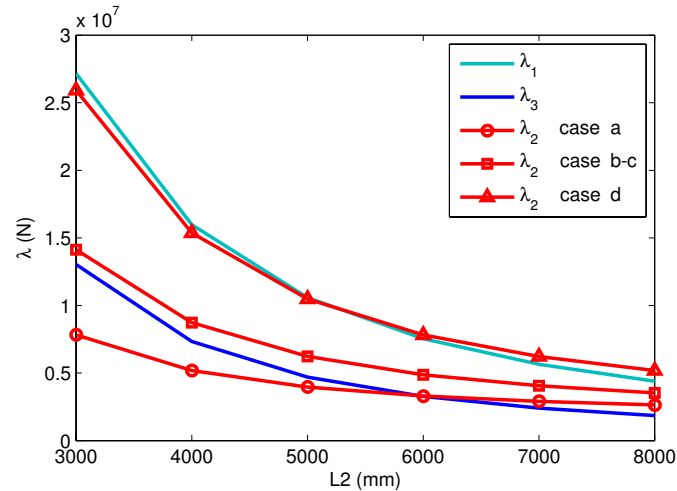


Figure 15. Critical loads versus column length for HEA240 bars.

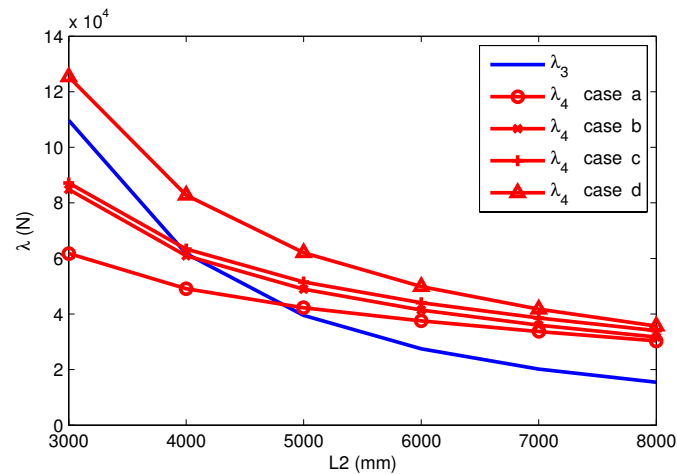


Figure 16. Critical loads versus column length for U100 bars.

cross-sections, respectively. The critical loads corresponding to modes 1 and 3 above are drawn in light blue and dark blue, respectively. The critical loads corresponding to modes 2 and 4 are drawn in red.

It is apparent that the flexural critical loads are not influenced by the constraints on warping as was to be expected. It also appears that the torsional mode has a significant effect on the critical load when the column is short.

In addition, Figure 15 shows that for the boundary conditions of case a $\lambda_2 < \lambda_3$ when $L_2 < 6000$ mm, that is, the purely torsional critical load is attained before the one corresponding to the buckling mode 3. Moreover, $\lambda_3 < \lambda_1$ for all L_2 ; this means that the critical load of the out-of-plane buckling mode is always lower than the one associated with the purely in-plane flexural, Euler-like, buckling mode. This sounds adequate, because in mode 3 the column bends around the lower inertia axis, while in the purely flexural mode 1 both the beam and the column bend around the axis of higher inertia which is twice the inertia

around the other axis. All the results show that when warping constraints are introduced at the ends of the bars, the flexural-torsional critical loads show a remarkable increase due to a globally stiffer system.

The analysis carried out after the introduction of the additional warping constraints labeled as cases b and c gives more or less the same results and one finds that $\lambda_3 < \lambda_2 < \lambda_1$. Finally, for the warping constraints of case d the critical load corresponding to the purely torsional mode attains the highest values and $\lambda_3 < \lambda_2 < \lambda_1$; only when $L_2 > 5200$ mm, that is, for very slender columns, the effect of the warping constraint is less significant and the out-of-plane mode 3 prevails on the purely torsional mode 2.

The dependence of the critical loads on the length L_2 of the column when the frame is composed of U100 bars is shown in Figure 16. It is first to be remarked that in this case only two buckling modes (modes 3 and 4) are possible, thus only two buckling loads henceforth denoted by λ_3 and λ_4 shall be calculated for the warping constraint cases a–d. From Figure 16 we deduce that we face the following different situations:

- $L_2 < 4000$ mm $\Rightarrow \lambda_4 < \lambda_3$ for cases a, b, and c. This is reasonable, since mode 4 is dominated by the very modest torsional stiffness of the channel. Moreover, the additional constraints for the warping do not seem to add enough stiffness to the system;
- 4000 mm $< L_2 < 4800$ mm $\Rightarrow \lambda_4 < \lambda_3$ for case a and $\lambda_3 < \lambda_4$ for cases b and c. That is, if the column becomes appreciably slender the mixed flexural-torsional mode for the column is attained at a lower critical load than the corresponding out-of-plane flexural mode when the warping constraints are not present. Even a modest set of additional warping constraints makes the opposite hold. This is reasonable since for slender bars the Euler flexural buckling load sensibly decreases, while even a modest increase in the torsional stiffness can make the mixed flexural-torsional buckling load increase over the purely flexural one;
- $L_2 > 4800$ mm $\Rightarrow \lambda_3 < \lambda_4$ for cases a, b, and c. This sounds again adequate since for very slender columns the Euler buckling load is so low that it is attained before any possible flexural-torsional buckling load even when modest additional warping constraints are introduced;
- In case d, that is when the stiffest system with respect to torsion and warping is considered, $\lambda_4 > \lambda_3 \forall L_2$. That is, when the frame has the highest possible stiffness against torsion, the Euler-like buckling load is the lowest critical load and hence the most important in applications, irrespective of the length of the column.

It has to be remarked that these results may be of importance in applications since design against Euler buckling is a well-known subject in engineers' education while design against flexural-torsional buckling of thin-walled structures is still a debated topic.

4. Final remarks

The direct one-dimensional beam model suitable for the description of the flexural-torsional buckling introduced in [Ruta et al. 2006] has been used to study two cases of interest in applications, namely a compressed beam with an intermediate stiffener and the Roorda frame. The direct formulation has made it possible to use standard static perturbation techniques of well-known reliability and to limit the use of numerical codes to the parametric solutions of the field equations for the buckling. Some very interesting results have been found which may have some importance in applications: the introduction

of an intermediate stiffener globally increases the stiffness of the beam against warping and torsion and makes the Euler buckling mode the most meaningful one. In the Roorda frame, the warping constraints and the length of the column play a very important role and the first critical load may sometimes not be the one corresponding to the Euler-like buckling mode. This fact of course is of interest in applications because of the well-known low torsion rigidity of thin-walled open sections. These results, to the authors' knowledge, are new and subject to further improvement. As a matter of fact, it appears that a further step in this study is the analysis of more complex 3D frames.

References

- [Bažant and Cedolin 1991] Z. P. Bažant and L. Cedolin, *Stability of structures: elastic, inelastic, fracture, and damage theories*, Oxford Engineering Science Series **26**, Oxford University Press, New York, 1991.
- [Budiansky 1974] B. Budiansky, "Theory of buckling and post-buckling behavior of elastic structures", *Adv. Appl. Mech.* **14** (1974), 1–65.
- [DiCarlo 1996] A. DiCarlo, "A non-standard format for continuum mechanics", pp. 263–268 in *Contemporary research in the mechanics and mathematics of materials: Symposium on Recent Developments in Elasticity, ASME Mechanics and Materials Conference* (Baltimore, MD, 1996), edited by R. C. Batra and M. F. Beatty, CIMNE, Barcelona, 1996.
- [Grimaldi and Pignataro 1979] A. Grimaldi and M. Pignataro, "Postbuckling behavior of thin-walled open cross-section compression members", *Mech. Based Des. Struct. Mach.* **7**:2 (1979), 143–159.
- [Gu and Chan 2005] J.-X. Gu and S.-L. Chan, "A refined finite element formulation for flexural and torsional buckling of beam-columns with finite rotations", *Eng. Struct.* **27**:5 (2005), 749–759.
- [Kim and Kim 2000] S.-B. Kim and M.-Y. Kim, "Improved formulation for spatial stability and free vibration of thin-walled tapered beams and space frames", *Eng. Struct.* **22**:5 (2000), 446–458.
- [Kim et al. 2001] M.-Y. Kim, S.-P. Chang, and H.-G. Park, "Spatial postbuckling analysis of nonsymmetric thin-walled frames, I: Theoretical considerations based on semitangential property", *J. Eng. Mech. (ASCE)* **127**:8 (2001), 769–778.
- [Koiter 1945] W. T. Koiter, *Over de stabiliteit van het elastisch evenwicht*, Ph.D. thesis, Delft, 1945. Translated in NASA TT F-10 vol. 833 (1967) and AFFDL Report TR 70-25 (1970).
- [Møllmann 1986] H. Møllmann, "Theory of thin-walled beams with finite displacements", pp. 195–209 in *Finite rotations in structural mechanics: proceedings of the Euromech Colloquium 197* (Jabłonna, 1985), edited by W. Pietraszkiewicz, Lecture Notes in Engineering **19**, Springer, New York, 1986.
- [Pignataro and Ruta 2003] M. Pignataro and G. C. Ruta, "Coupled instabilities in thin-walled beams: a qualitative approach", *Eur. J. Mech. A Solids* **22**:1 (2003), 139–149.
- [Pignataro et al. 1991] M. Pignataro, N. L. Rizzi, and A. Luongo, *Stability, bifurcation and postcritical behaviour of elastic structures*, Elsevier, Amsterdam, 1991.
- [Pignataro et al. 2006] M. Pignataro, N. L. Rizzi, and G. C. Ruta, "Buckling and post-buckling in a two-bar frame: a qualitative approach", pp. 337–346 in *4th International Conference on Coupled Instabilities in Metal Structures (CIMS 2004)* (Rome, 2004), edited by M. Pignataro et al., Tipografia Esagrafica, Rome, 2006.
- [Reissner 1983] E. Reissner, "On a simple variational analysis of small finite deformations of prismatical beams", *Z. Angew. Math. Phys.* **34**:5 (1983), 642–648.
- [Rizzi and Tatone 1996] N. Rizzi and A. Tatone, "Nonstandard models for thin-walled beams with a view to applications", *J. Appl. Mech. (ASME)* **63**:2 (1996), 399–403.
- [Ruta et al. 2006] G. Ruta, M. Pignataro, and N. Rizzi, "A direct one-dimensional beam model for the flexural-torsional buckling of thin-walled beams", *J. Mech. Mater. Struct.* **1**:8 (2006), 1479–1496.
- [Ruta et al. 2008] G. C. Ruta, V. Varano, M. Pignataro, and N. L. Rizzi, "A beam model for the flexural-torsional buckling of thin-walled members with some applications", *Thin-Walled Struct.* **46**:7–9 (2008), 816–822.
- [Simo and Vu-Quoc 1991] J. C. Simo and L. Vu-Quoc, "A geometrically-exact rod model incorporating shear and torsion-warping deformation", *Int. J. Solids Struct.* **27**:3 (1991), 371–393.

- [Tatone and Rizzi 1991] A. Tatone and N. Rizzi, "A one-dimensional model for thin-walled beams", pp. 312–320 in *Trends in applications of mathematics to mechanics* (Hollabrunn, 1989), edited by W. Schneider et al., Longman, Harlow, 1991.
- [Teh 2005] L. H. Teh, "Spatial rotation kinematics and flexural-torsional buckling", *J. Eng. Mech. (ASCE)* **131**:6 (2005), 598–605.
- [Timoshenko and Gere 1961] S. P. Timoshenko and J. M. Gere, *Theory of elastic stability*, McGraw-Hill, New York, 1961.
- [Truesdell and Noll 1965] C. Truesdell and W. Noll, *The non-linear field theories of mechanics*, Handbuch der Physik **III/3**, Springer, Berlin, 1965.
- [Vlasov 1961] V. Z. Vlasov, *Thin-walled elastic beams*, Monson, Jerusalem, 1961.

Received 3 Dec 2008. Revised 28 Apr 2009. Accepted 19 Jun 2009.

MARCELLO PIGNATARO: marcello.pignataro@uniroma1.it

Dipartimento di Ingegneria Strutturale e Geotecnica, Università degli Studi di Roma 'La Sapienza', via Eudossiana 18, 00184 Roma, Italy

NICOLA RIZZI: nlr@uniroma3.it

Dipartimento di Strutture, Università degli Studi Roma Tre, via Corrado Segre 6, 00146 Roma, Italy

GIUSEPPE RUTA: giuseppe.ruta@uniroma1.it

Dipartimento di Ingegneria Strutturale e Geotecnica, Università degli Studi di Roma 'La Sapienza', via Eudossiana 18, 00184 Roma, Italy

VALERIO VARANO: v.varano@uniroma3.it

Dipartimento di Strutture, Università degli Studi Roma Tre, via Corrado Segre 6, 00146 Roma, Italy

